

Some Peculiarities the Modeling the Surface Processes of Relaxed Optics

Petro P. Trokhimchuck *

Anatoliy Svidzinskii Department of Theoretical and Mathematical Physics, Lesya Ukrayinka East European National University, Lutsk, Ukraine

***Corresponding Author:** Petro P. Trokhimchuck, Anatoliy Svidzinskii Department of Theoretical and Mathematical Physics, Lesya Ukrayinka East European National University, Lutsk, Ukraine

Abstract: Basic peculiarities of modeling the surface processes of Relaxed Optics are discussed. Main experimental data for various materials and regimes of laser irradiation are represented and analyzed. It was shown that these processes may be having nonequilibrium and irreversible nature. Bond between radiated and non-radiated relaxation or processes of Nonlinear and Relaxed Optics is observed. Physical-chemical and electrodynamics' aspects of these phenomena are analyzed. Vladimir Makin model of surface polariton-plasmon and cascade model of excitation of proper chemical bonds in the regime of saturation the excitation are used for the explanation of the presented experimental data for all solids, including polymers.

Keywords: Relaxed Optics, surface processes, saturation of excitation, cascade processes, irreversible phenomena, Vladimir Makin model, polymers, semiconductors, metals.

1. INTRODUCTION

Problem of modelling surface processes of Relaxed Optics (RO) is connected with problem of increasing lifetime of basic elements of optoelectronic systems, including semiconductors, optical fibers and other [1 – 4].

In whole this problem [1 – 4] is very complex problem. It connected with various nature of relaxation of first-order optical excitation. It may be simple two-three-stage, cascade, cyclic or more complex relaxation. Processes of radiative and nonradiative relaxation generally interconnected, they cause each other. First (radiative) processes are processes of Nonlinear Optics (NLO) [5]. Second (nonradiative) processes are processes of Relaxed Optics. Therefore we must use various old methods and create new methods of modeling of these processes and phenomena.

Basic experimental data of a creation the surface and subsurface laser-induced structures are next: creation surface frozen interferograms with various spatial periods; creation the nanohills or microcolumns (structures of soliton type with heights from 10 nm to 50 μm). These structures created on various materials from metals and semiconductors to glasses and polymers [6 – 22].

Modeling of these processes must include two basic aspects. First, electromagnetic, which is can explain the basic peculiarities of creation the surface laser-induced ripples (interferograms). This part of experimental data may be explain with help Vladimir Makin model of surface polariton-plasmons [7]. Second, physical-chemical, which can explain of the irreversible nature the ripples and other surface laser-induced interferograms. This part of experimental data may be explained with help of various physical-chemical models, includinf modified model of photoelectric effect, one and two-diffusive models, cascade model of excitation the proper chemical bonds in the regime of saturation the excitation, models of laser-induced ablation and other. In addition proper phenomenological models may be used for the observation some peculiarities of these processes.

Methods of Relaxed Optics allow to observe self-absorption processes in various solid and to add methods of Linear and Nonlinear Optics, which are accent the attention on photoelectric effect or determination the absorption band edge.

Really Relaxed Optical Processes have cascade nature and therefore we must take into account this fact for modeling of proper processes.

In this paper we accent attention on the creation surface laser-induced ripples and other structures only. Other experimental data and its explanation are represented in [1 – 2].

2. EXPERIMENTAL DATA

First experimental data of irreversible interaction the laser radiation and semiconductors were received by M. Birnbaum in 1965 [19]. He observed the surface interferograms after pulse Ruby-laser irradiation of germanium, silicon, indium antimonite a.o. [19]. These results are beginning of researches of surface laser-induced phase transformations.

More detail research of creation the surface laser-induced structures are represented by A. Medvid' in [6]. Surfaces nanostructures were received after irradiation of SiO_2/Si structure by second harmonic Nd:YAG laser at density of power $I = 2.0 MW/cm^2$, pulse duration 10 ns, wavelength 532 nm and frequency of repetition 12,5 Hz [6]. These structures (nanohills) had heightb 10-15 nm.

Samples of Ge {111} and Ge {001} i-type single crystals are used in experiment. Nd:YAG laser (wavelength 1,064 μm , duration of pulse 15 ns, pulse rate 12,5 Hz, power P=1 MW) was used for the irradiation. The AFM picture of Ge surface after Nd laser irradiation is represented in Fig. 1 [6]. In this case nanostructures had height ~ 200 nm.

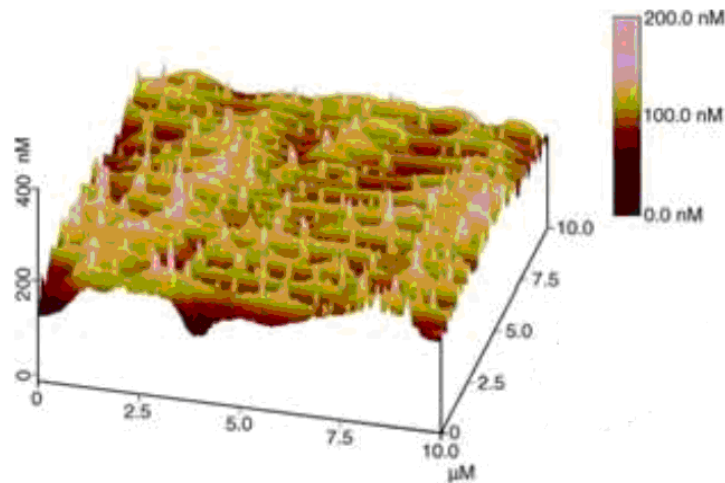


Fig1. Three-dimensional AFM image of nanostructures after Nd:YAG laser irradiation with density of power 28 MW/cm^2 on Ge surface [6].

More large columns (height 20 μm , diameter 2 – 3 μm) were received after irradiation of pulse series the nanosecond eximer KrF-laser (wavelength 248 nm, pulse duration 25 ns) (Fig. 2.). This figure illustrates the high aspect ratio silicon micro-columns that were formed in air after 1000 laser shots at an energy density, E_d , between 2.7 and 3.3 J/cm^2 . The columns are $\sim 20 \mu m$ long and $\sim 2\sim 3 \mu m$ in diameter. Moreover, surface-height profilometry performed using a Dektak II profiler revealed that most of the length of the microcolumns, 10 – 15 μm , protrudes above the original Si surface [8, 9]. The microcolumn morphology changes if the atmosphere is changed during laser irradiation. Fig. 2 b) shows several columns in a specimen that was first irradiated with 600 pulses in air and 1200 pulses in $N_2/5\%O_2$ [8, 9].

The importance of the gas environment was emphasized, when a plasma etchant, SF_6 , was used as the ambient gas during laser irradiation of silicon [8, 9]. In SF_6 extremely long structures are produced that look at first like walls surrounding very deep central holes (see Fig. 2 c)) [8, 9].

Ordered laser-induced nanostructures, which were created on surface of Si after laser irradiation ($\lambda = 0,8 \mu m$, $\tau_i = 100$ fs, number of pulses 200) through lay of water (Fig. 3) [10]. Three types of micro and nanostructures are generated [109]. Nanostructures have typical spatial scale $d_1 = 600$ nm and $d_2 = 120$ nm, here lattice vector oriented $\vec{g} \parallel \vec{E}$. It is corresponded to interference between surface polariton-plasmon (SPP) and TM electromagnetic wave [7]. Structures with period d_1 are generated for interference of falling wave with SPP wave, which arise on the border water – free electrons of silicon. Structures with period d_2 are generated for mutual interference of two SPP, which were propagated in mutually inverse directions along border silicon – plasmic layer. Structures with period 120 nm aren't depended from nature of liquid, which was contacted with silicon [7, 10]. It is experimental fact.

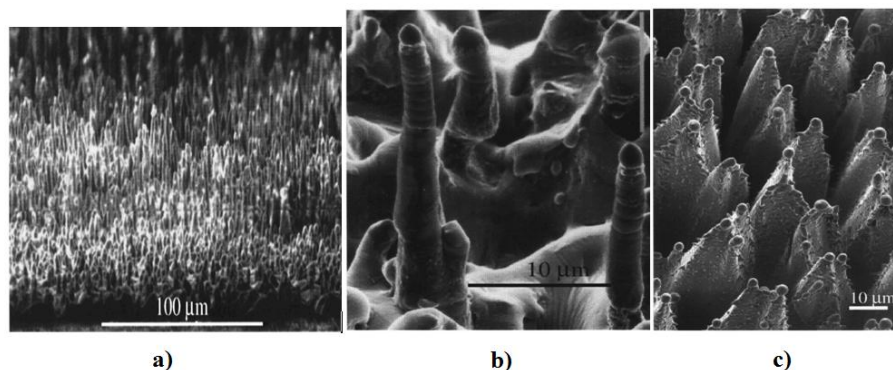


Fig2. a) SEM images of silicon microcolumns after 1000 laser shots in air at $E_d = 3 J/cm^2$ [129]; b) SEM image showing a change in Si microcolumn morphology controlled by the ambient gas composition at $E_d 2.7 J/cm^2$. The arrows indicate the height achieved after 600 laser pulses in air ($N_2 - 18\% O_2$); the remainder of the columns was grown by 1200 laser pulses in $N_2 - 5\% O_2$ [129]. c) Walled Si structure produced by 2040 laser pulses at $E_d = 1.5 J/cm^2$ in 1 atm of SF_6 [8, 9].

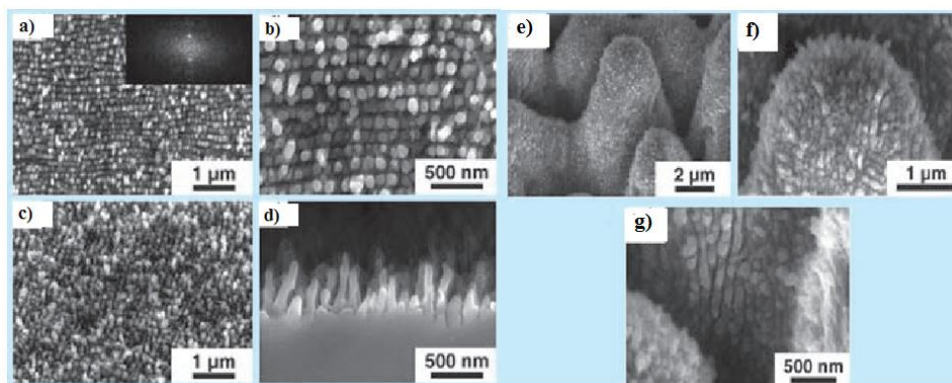


Fig3. Nanocolumns, which are generated after irradiation structures of silicon with $d_2=120$ nm, (wavelength of irradiation 800 nm, number of pulses – 200, density of energy of irradiation $0,5 kJ/m^2$): a) and b) turn of polarization on 90° , c) turn of polarization on 45° , d) cross chip of nanocolumns. On insertion to Fig. 2.8a – Fourier-picture of structures [157]. e) – g) Surface silicon nanocolumns of little scale, which have orthogonal orientation to a crests of nanorelief of large scale [10].

Laser-induced silicon nanostructures ($\lambda = 0,8 \mu m$, $\tau_i = 100$ fs, number of pulses 200) with $d_3=90$ nm, which was generated after irradiation structures of changing polarization with $d_2=120$ nm, when orientation of vector \vec{E} was changed on 90° relatively to initial action. Power of laser irradiation was less in two time as for initial structure. Generated periodical structures are nanocolumns with height to 400 nm with spatial period 90 nm and orientation wave vector $\vec{g} \parallel \vec{E}$ [7, 10]. Where \vec{g} is beam propagation direction.

Generation of periodical nanostructures along crests ($d=90$ nm) is cause with interference of falling radiation with surface polaritons, which are exited along crest of relief ($d \sim 120$ nm), and with mutual interference of surface polariton-plasmons [7]. A crest of relief, which considered in contact with the substrate, was selected as initial half-cylinder. Formed in this case inoculating regular relief $d \sim 90$ nm is basis for further growth of nanocolumns. Since typical radius of half-cylinder $r \ll \lambda$, therefore dispersion relation for surface polariton-plasmon in cylindrical geometry is changed from dispersion relation in plane geometry of phase separation. It cause to formation nanostructures with less period as for plane case [7].

For case of elliptic polarization and falling angle to surface from 0 to 20° basic nanostructures are created: 1) surface nanostructures with period ~ 200 nm and 2) these structure with period 70–100 nm are generated on crest of structure 1, but its orientation $\vec{g} \perp \vec{E}$ [7].

The influence of number fs-pulses Ti:sapphire laser on parameter of surface silicon structures is observed in [11]. Laser radiation ($\lambda = 800$ nm, $\tau = 100$ fs, $\nu = 1$ kHz) was focused onto a spot of about

100 μm diameter and had intensity below the single shot ablation threshold of $2 \cdot 10^{12} \text{ W/cm}^2$. Irradiation was made by series of 10000, 20000 and 120000 pulses. Maximal height of surface structures was $\sim 7 \mu\text{m}$ [11].

Basic difference between nanosecond and femtosecond regimes of creation of surface silicon nanostructures is the its sizes: 15-20 nm for nanosecond regime of irradiation (nanohills) for Neodymium laser [6], 20 – 50 μm for eximer laser (Fig. 3) and 400-450 nm for femtosecond regime of irradiation (Fig. 4). These data are proved electromagnetic mechanisms of creation surface nanostructures (surplus of negative charge is caused the electromagnetic swelling of surface) [1, 2]. Heat processes are caused the decrease of sizes, including height of surface nanostructures. But we have nanosecond laser-generated silicon microstructures [6] and 200 nm germanium nanostructures (Fig. 1), which are shown an influence of intensity and mechanisms of light absorption and number of pulses on the generation surface structures.

For the modeling processes of Fig. 3 we must develop electromagnetic concept of RO. This concept allows including in parametric optical processes back side of “medal”: resulting trace of interaction light and matter in matter [1, 2].

An influence of pulses number on the processes of formation of laser-induced periodic nanostructures on titanium plate is observed in [13, 14]. Sapphire laser system was used for the irradiation. It had next parameters: wavelength 800 nm , repetition rate 1 kHz , pulse length 100 fs , beam diameter 4 mm and density of energy of irradiation 0,25; 0,75 and 1,5 J/cm^2 . Interference structures are generated for the irradiation with energy density 0,25 J/cm^2 [13]. Evolution of creation laser-induced surface structures, the period of the parallel periodic microstructures as a function of the number of laser pulses, a distance between the microdots along the hill of periodic microstructures as a function of the number of laser pulses and a phenomenon of doubling of period of laser-induced surface structures were observed in [13]. As shown in [13], the period was gradually increased in the range of 10–70 pulses and increased in the range of 70–110 pulses as the number of pulse increased. A distances between the microdots along the hill of periodic microstructures as a function of the number of laser was increased in the range of 50–110 pulses. But these distances are correlated with height and width of interferogram bands [13].

Analogous laser-induced phase transformations martensite-austenite in AISI H13 were received in [18]. The parameter of CO_2 -laser irradiation were next (wavelength 10,6 μm , density of power $1,02 \cdot 10^9 \text{ W/m}^2$, sizes of focused laser spots were 0, 09, 0,2 and 0,4 mm). The maximal value of hardness was received for the irradiation of spot 0,4 mm .

Experimental data for receiving femtosecond periodical laser-induced surface structures (LIPSS) for low-spatial frequency (LSFL) and high-spatial frequency (HSFL) for various matter were received in [15, 16]. Irradiation was realized with help Ti:sapphire laser amplifier system with linearly polarized laser pulses of $\tau = 30 - 150 \text{ fs}$, wavelength 790 – 800 nm and pulse repetition from 10 Hz to 1 kHz . Three different materials (titanium, silicon and fused silica) were irradiated [15].

Dependence of LSFL spatial period as a function of number laser pulses for the silicon and LSFL spatial period Λ_{LSFL} in fused silica upon double fs-pulse irradiation were observed in [15].

Literature survey of LIPSS reported on inorganic solids upon near-infrared fs-laser pulse irradiation ($\lambda \sim 740 - 800 \text{ nm}$, $\tau = 25 - 160 \text{ fs}$, $\nu \leq 5 \text{ kHz}$) under nearly normal incidence in air or vacuum are represented in [15].

Ti:sapphire laser system (KMLabs Inc.) with a central wavelength of 800 nm , a pulse duration of 100 fs , number of pulses 450 and 1400, density of irradiation energy 5, 7 and 8,6 kJ/m^2 and a repetition rate of 5 kHz for irradiation the silicon in two employed ambient media (air and isopropanol) was used in [17]. The comparison of the structure shapes resulting from air and isopropanol was observed. The maximal value the heights of laser-induced surface structures were 10-19 μm in air and 2-6 μm in isopropanol. Correlations of remaining substrate thickness and structure height for different number of pulses are observed too.

The laser-induced periodical structures were received in polymer structures two. For many polymer surfaces (including polyethylene terephthalate (PET), polyimide (PI) and polystyrene (PS)) organized

LSFL nano-triple structures surfaces can be induced by irradiation with pulsed UV lasers with laser pulse length in the order of some nano-seconds at fluences well below the ablation threshold and with a large number of laser pulses (typically about 5000). It was found that the periodicity and the height of the structures depend on the laser wavelength λ as well as the angle of incidence θ of a laser beam. For s-polarization, the lateral periodicity Λ is given by [20 – 22]

$$\Lambda = \frac{\lambda}{n_{eff} - \sin \theta}. \quad (1)$$

The minimal value of Λ can be calculated by the laser wavelength λ divided by the effective index of refraction n_{eff} , which lies between the refractive index of air (=1) and refractive index of polymer (typically $\sim 1,5$). The direction of the ripples on PET is parallel to the direction of the polarization. The smallest features of this kind reported so far were produced by our group by 157 nm F₂ excimer laser irradiation of PET foils. Typical examples of this irradiation are represented in Fig. 4 [22]. The period of the ripples depends on the laser wavelength and the angle of incidence of the radiation according formula (1).

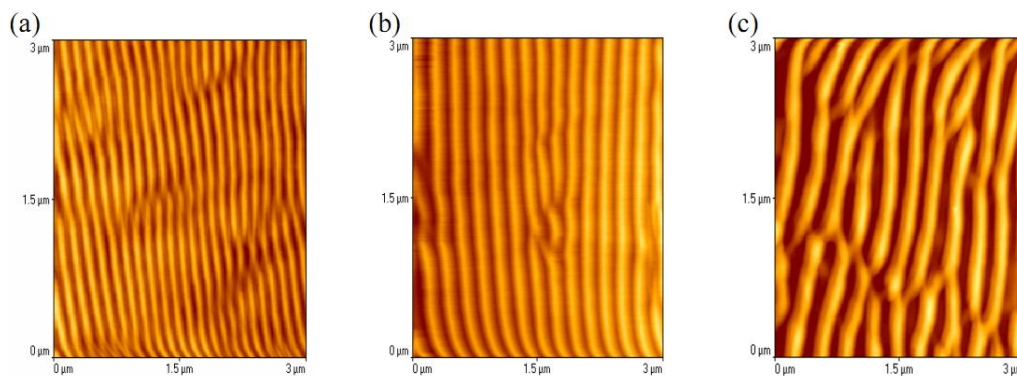


Fig4. LSFL-type ripples on polymer surfaces induced by nano-seconds laser irradiation: AFM images of $\lambda = 157$ nm F₂ induced ripples at PET irradiated under angle θ of (a) 0°, (b) 22,5° and (c) 45°. Ripple period Λ is about 140 nm, 195 nm and 240 nm and ripple height about 30 nm, 50 nm and 95 nm respectively [22].

Femtosecond laser irradiation ($\lambda = 248$ nm, $\tau = 500$ fs) was used for irradiation the polymers PI and PET. These results are represented in Fig. 5.

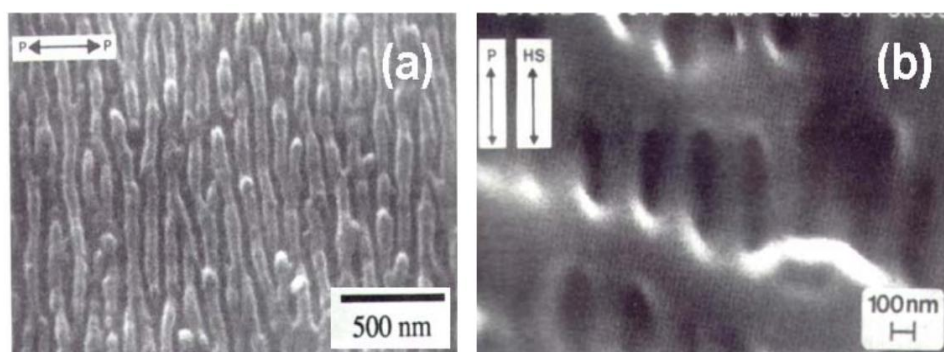


Fig5. HSFL-type ripples on polymer surfaces by femtosecond laser irradiation: electron microscope images of surface structures on (a) PI irradiated with a 500 fs 248 nm KrF laser beam at a fluence $\phi = 14$ mJ/cm² and $N = 60$ laser pulses and (b) PET with $\phi = 79$ mJ/cm² and $N = 5$. The arrows P indicate the direction of the laser light polarization [22]

An influence of intensity and number pulses of irradiation on formation the surface nanostructures on polymer films PVDF and PTT for the linear and circular polarization is presented in [21]. Regime of irradiation was next: fourth and fifth harmonics of Nd-laser (pulse duration 6 ns, repetition rate 10 Hz) [20], Laser irradiation is increased the sizes of crystal fractures in semicrystalline films of PVDF (Fig. 6 (a) – (c)) and generated crystal structures in amorphous PTT (Fig. 6 (d) – (f)).

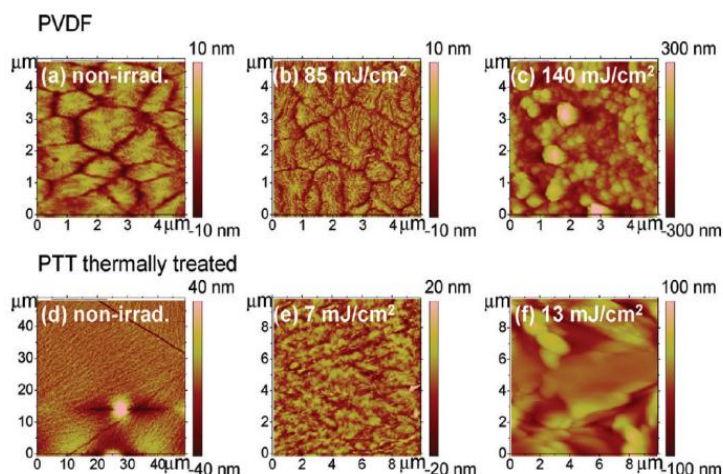


Fig6. An influence of polarization on formation the surface nanostructures on polymer films for the linear and circular polarization [20].

Data of Fig. 5 and [7, 20, 21] show the dependence of formation the picture of surface laser induced structures from polarization the radiation as for semiconductors, metals and glasses [1, 2].

3. MODELING AND DISCUSSIONS

For the explanation of experimental data, which are represented in 2.2, we must estimate all possible mechanisms of relaxation: kinetic and dynamical; and possible mechanisms of excitation: hierarchical photo ionization. In this case we must include respective chain of relaxation times [174, 194]. It is necessity for the more full representation and modeling real and possible physical processes for the respective regimes of interaction.

Thus this representation of the modeling dangling bonds, which are created with help laser irradiation, is very effective method. It allows including in consideration effects of equilibrium, nonequilibrium and irreversible relaxations [1, 2].

Now we show the using of cascade model for the explanation experimental data of laser-induced phase transformations in silicon, germanium, carbon and titanium. It was called as case the structural phases.

The question about the influence of saturation of excitation on effects of RO may be represented as process of transitions between stable and metastable phases too. Now we'll estimate the influence of parameters of irradiation (including spectral) on irreversible changes and transformations in *Si* and *Ge*. Spectral dependences of absorbance of various structural modification of *Si* are represented in [1, 2]. Now we'll be estimated intensities of eximer, Ruby and Neodymium laser irradiation (wavelengths of irradiation are 0,248 μm , 0,69 μm and 1,06 μm properly of silicon and germanium, which are necessary for the creation of proper irreversible changes in irradiated semiconductor. As shown in [1, 2], absorbance of the Neodymium laser radiation in silicon is equaled 100 cm^{-1} , second harmonic of Neodymium laser – 10^4 cm^{-1} , eximer laser – 10^6 cm^{-1} .

Crystal semiconductors *Si* and *Ge* have, basically, the structure of diamond. Volume atomic density of elementary lattices may estimate according to formula [1, 2]

$$N_a = \frac{\rho N_A}{A}, \tag{2}$$

where ρ – density of semiconductor, N_A – Avogadro number, A – a weight of one gram-atom. For *Si* $N_{aSi} = 5 \cdot 10^{22}\text{ cm}^{-3}$, and for *Ge* $N_{aGe} = 4,4 \cdot 10^{22}\text{ cm}^{-3}$.

But *Si* and *Ge* may be crystallized in lattices with hexagonal, cubic, trigonal and monoclinic symmetry. Phase diagram of Si as function of coordination number is represented on Fig. 7 [23].

Coordination number (CN) 8 is corresponded of diamond lattice, CN 6 – hexagonal lattice, (CN) 4 and (CN) 3 – other two lattices. It should be noted that melting temperatures of these phases are various. Volume density of CN is equaled $\text{CN} \cdot N_a$. For diamond symmetry of lattice this value is $8N_a$.

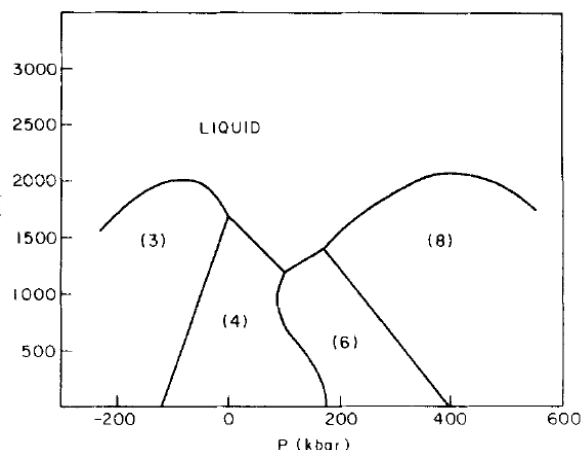


Fig7. A schematic phase diagram for Si(CN). The coordination numbers (CN) of the various phases are indicated. The diagram is based on common features of the phase diagrams of column IV elements as described by the references cited in Pistorius's review (Ref. 8 in [15]). Starting from a high temperature $>3 \times 10^3 K$ and subject to a constraint of average density $\langle \rho \rangle = \rho(4)$, a hot micronucleus will tend to bifurcate into the most stable phases (highest T_m) which straddle Si(4) in density. These are Si(3) and Si(8), as indicated by the diagram [23].

Roughly speaking, transition from one phase to another for regime of saturation of excitation may be modeled as one-time breakage of proper numbers of chemical bonds, which are corresponded to the difference of CN of proper phases. For example, two bonds breakage is caused the phase transition from diamond to hexagonal structure. One bond breakage in the regime of saturation is caused to generation of laser radiation.

Results of calculation of volume densities of energy, which are necessary for breakage of proper number of bonds in regime of saturation of excitation, are represented in Table 1 [1, 2].

Table1. Volume density of energy I_{vi} ($10^3 J/cm^3$), which is necessary for the breakage of proper number of chemical bonds in the regime of saturation of excitation in Si and Ge.

Material	I_{v1}	I_{v2}	I_{v4}	I_{v5}
Si	12,8 – 14,4	25,6 – 28,8	51,2 – 57,6	63 – 72
Ge	6,3 – 8,4	12,6 – 16,8	25,2 – 33,6	31,5 – 42

It conceded that energies of all chemical bonds for elementary lattice are equivalent (Si and Ge are pure homeopolar semiconductors) [1]. For silicon energy of covalent bonds Si-Si are equaled 1,2–1,8 eV; for germanium energy of covalent bonds Ge-Ge are equaled 0,9–1,6 eV. Minimal values of these energies are corresponded of Pauling estimations. These values are corresponded the energy on one CN: according to radiation physics of status solid Zeits energy of creation one radiation defect in silicon is equal 12,7 eV for diamond lattice [1, 2].

Surface density of energy on proper numbers of CN for proper lasers irradiation may receive after division of results of Table 1 on proper absorbance. This procedure allows to transit from bulk to surface density of energy, which is necessary for the receiving of proper phenomena. Results of these calculations are represented in Table 2 [1, 2].

It should be noted that real regimes of irradiation must be more (process of light reflection wasn't included in our estimations). In addition we aren't include the relaxation (time) processes for the scattering of light on stable centers (self-absorption in crystals) as for InSb and InAs [2-4].

Table2. Surface density of energy I_{si} (J/cm^2), which are necessary for the breakage of proper numbers of chemical bonds in Si and Ge crystals after proper lasers irradiation in regime of saturation the excitation [1, 2]

	I_{s1}	I_{s2}	I_{s4}	I_{s5}
Si, 1,06 μm	128 – 144	256 – 288	512 – 576	630 – 720
Si, 0,53 μm	1,28 – 1,44	2,56 – 2,88	5,12 – 5,76	6,3 – 7,2
Si, 0,248 μm	0,0128 – 0,0144	0,0256 – 0,0288	0,0512 – 0,0576	0,063 – 0,072
Ge, 1,06 μm	0,63 – 0,84	1,26 – 1,68	2,52 – 3,36	3,15 – 4,2
Ge, 0,53 μm	0,32 – 0,42	0,63 – 0,84	1,26 – 1,68	1,58 – 2,1

Remark to Table 2: absorbencies of Si (Neodimium laser) – 100 cm^{-1} ; Si (second harmonic of Neodimium laser) – $\sim 10^4 \text{ cm}^{-1}$; Si (eximer laser) – $\sim 10^6 \text{ cm}^{-1}$. Ge (Neodimium laser) – $\sim 10^4 \text{ cm}^{-1}$; Ge (second harmonic of Neodimium laser) – $2 \cdot 10^4 \text{ cm}^{-1}$.

Height of surface nanostructures for the nanosecond regime of irradiation is maximal (200 nm, Fig. 1) for the germanium [6] for small number of pulses and for silicon (20 – 50 μm , Fig. 2) for large number of pulses [8, 9]. For the silicon, which was irradiated by one pulse of Nd-laser [6] height of laser-generated surface nanostructures is change from 10 nm to 20 nm. This difference can be explained in next way. Index of light absorption with wavelength 532 nm of Ge crystal with diamond symmetry is more as silicon with this symmetry for the nanosecond irradiation. But surface part of irradiated germanium is transited to hexagonal phase. It is experimental data. Other result given's phase transitions. The hexagonal lattice of germanium has greater size as diamond modification. Therefore hexagonal nanostructures are greater and more stable as polycrystalline or metallic nanohills.

The qualitative explanation of possible mechanisms of creation microcolumns or nanohills may be determined with help next model. We can determine the change of the height and volume of corresponding structural unit on pulse. This procedure may be used for the comparative regimes of irradiation. Now we are demonstrated this method for silicon. Results of these estimations are represented in Table 3 and Table 4 [1].

Table3. Geometrical characteristics of laser-induced surface structures (microcolumns and nanohills)

Material	λ_{ir}, nm	Height	V_{con}	V_{cyl}	ΔV_{con}	ΔV_{cyl}	Ref.
e	1064	200 nm	32054 nm ³	31400 nm ³	157 nm ³	160 nm ³	[6]
Si	248	30 μm	282,6 μm^3	288,5 μm^3	0,236 μm^3	0,240 μm^3	[8, 9]
Si	248	50 μm	11775 μm^3	11343 μm^3	5,77 μm^3	5,56 μm^3	[8, 9]
Si	800	400 nm	20933 nm ³	22608 nm ³	52,33 nm ³	56,52 nm ³	[10]
Si	800	7 μm	1,1 μm^3	1,2 μm^3	$5.1 \cdot 10^{-4} \mu\text{m}^3$	$5.7 \cdot 10^{-4} \mu\text{m}^3$	[17]
PI polimer	248	1000 nm	$1.9 \cdot 10^6 \text{ nm}^3$	$2.0 \cdot 10^6 \text{ nm}^3$	$3.2 \cdot 10^4 \text{ nm}^3$	$3.3 \cdot 10^4 \text{ nm}^3$	[22]

Table4. Geometrical characteristics of laser-induced surface structures (microcolumns and nanohills). Conic and cylindrical parameters

Material	λ_{ir}, nm	r_{con}	r_{cyl}	E_{s1}	Ref.
Ge	1064	20 nm	10 nm	1,32 pJ	[6]
Si	248	3 μm	1,75 μm	0,76 μJ	[8, 9]
Si	248	15 μm	8,5 μm	10,59 μJ	[8, 9]
Si	800	7 nm	4,25 nm	0,076 pJ	[10]
Si	800	0,43 μm	0,25 μm	3,3 nJ	[17]
PI polimer	248	43 nm	25 nm	813 fJ	[22]

Energy characteristics of laser-induced surface structures (microcolumns and nanohills) are represented in Table 5 [1].

Table5. Energy characteristics of laser-induced surface structures (microcolumns and nanohills)

Material	λ_{ir}	Height	E_{con}	E_{cyl}	ΔE_{con}	ΔE_{cyl}	Ref.
Ge	1064	200 nm	0,40-0,54 fJ	0,40-0,53 fJ	0,0020-0,0027 fJ	0,0020-0,0026 fJ	[6]
Si	248	30 μm	7,2-8,1 nJ	7,4-8,3 nJ	6,0-6,8 pJ	6,2-6,9 pJ	[8, 9]
Si	248	50 μm	0,30-0,34 μJ	0,29-0,33 μJ	0,15-0,17 nJ	0,14-0,16 nJ	[8, 9]
Si	800	400 nm	0,54-0,60 fJ	0,58-0,65 fJ	0,0013-0,0015 fJ	0,0014-0,0016 fJ	[10]
Si	800	7 μm	28,6-31,7 pJ	30,7-34,6 pJ	13,6-15,1 pJ	14,6-16,5 pJ	[17]

Mechanisms of creation other laser-induced nanostructures may be explained on the basis cascade model of step-by-step excitation of corresponding type and number of chemical bonds in the regime of saturation of excitation (Tables 1 and 2). According to this model decrease of symmetry of irradiated matter is occurred with increase of intensity of irradiation (Nd laser irradiation of silicon, germanium and carbon) [1, 2].

But in [6] the explanation of creation laser-induced hexagonal phase on germanium surface is based on the Benard phenomenon: generation of hexagonal phases in heated liquid on roaster. In our case heating of irradiated matter is generated in opposite direction from surface to deep and we have volume, but not surface as in Benard effect, structures. This effect is observed for few liquids. Rayleigh-Chandrasekar theory [24-26] is described this process as thermal-diffusive processes [6]. In this case we have transition from more low volume symmetry to more high surface symmetry. Chandrasekar created the hydromagnetic theory of creation sunspots [4]. Benar effect may be observed in other regimes of irradiation as in Fig. 1. For laser-induced creation volume hexagonal structures on *Ge* we have inverse transition: from high volume symmetry (diamond modification) to more volume low symmetry (hexagonal symmetry) [1, 2].

We can introduce criterion of efficiency the using of laser radiation for generation proper structures [1].

$$\Delta = \frac{E_{con(cyl)}}{E_{s1}} \tag{3}$$

Estimations of data Table 3 – Table 5 are represented in Table 6.

Table6. Efficiency of using the various regimes of laser irradiation for creation proper surface structures

Material	λ_{ir}	Δ_{con}	Δ_{cyl}	Ref.
Ge	1064	$3,0 \cdot 10^{-4} - 4,1 \cdot 10^{-4}$	$3,0 \cdot 10^{-4} - 4,0 \cdot 10^{-4}$	[6]
Si	248	$9,5 \cdot 10^{-3} - 10,6 \cdot 10^{-3}$	$9,7 \cdot 10^{-3} - 10,9 \cdot 10^{-3}$	[8, 9]
Si	248	0,028 – 0,032	0,029 – 0,031	[8, 9]
Si	800	$7,1 \cdot 10^{-3} - 7,9 \cdot 10^{-3}$	$7,6 \cdot 10^{-3} - 8,6 \cdot 10^{-3}$	[10]
Si	800	$8,7 \cdot 10^{-3} - 9,6 \cdot 10^{-3}$	$9,3 \cdot 10^{-3} - 10,5 \cdot 10^{-3}$	[17]

Relative efficiency of using laser irradiation for silicon for various regimes of irradiation may be determined with help next formula [1]

$$\eta = \frac{\Delta V_i}{\Delta V_{max}} \tag{4}$$

Relative efficiencies for silicon from data of Table 2.5 are represented in Table 7.

Table7. Relative efficiencies for silicon from data of Table 2.5.

Material	λ_{ir}	η_{con}	η_{cyl}	Ref.
Si	248	0,0432	0,0409	[8, 9]
Si	248	1	1	[8, 9]
Si	800	$10,2 \cdot 10^{-9}$	$9,1 \cdot 10^{-9}$	[10]
Si	800	$10,3 \cdot 10^{-5}$	$8,8 \cdot 10^{-5}$	[17]

On the basis of data of Tables 6 and 7 we can made next conclusions:

- 1) influence of wavelength irradiation on formation the nanohills and microcolumns: radiation of eximer laser is more effective as irradiation with wavelength 800 nm;
- 2) oxidation process of irradiated silicon is decreased the speed of generation the surface structures;
- 3) speed of generation the surface laser-induced structures is increased with increasing of number the pulses.

The mechanisms of light absorption are influenced on the relaxation time of excitation. Proper phenomenological chain of relaxation times is represented in [2]. The number of disrupt chemical bonds or CN may be determined with help next

$$n = 2 \ln \frac{h\nu}{E_a} \tag{5}$$

Where E_a – the energy of ionization (breakage) of proper bond.

Formula (5) is true for $h\nu > E_a$ only. For case with irradiation silicon by eximer laser with wavelength 248 nm or 5 eV n is equaled 3,2 [1].

More pure ionizing results were received for the irradiation silicon by femtosecond laser pulses in multipulse regime [1]. One quantum of eximer laser radiation may be ionized 3,2 chemical bonds according to formula (5). Therefore multipulse regime of the irradiation is caused the generation silicon structures with hexagonal and trigonal symmetry. Density of energy 2,7 J/cm² (Fig. 2a) and 1,5 J/cm² (Fig. 2 b) certificated this hypothesis. First regime (Fig. 2 a) allows receiving more thin and high structures with more low symmetry, which is stipulated more high intensity of irradiation. Second regime (Fig. 2 b)) may be results of generation the structures with more low symmetry (no cubic). Atmosphere of irradiation must be has influence on finishing picture. This conclusion is certificated by experimental data of Fig. 2 b) and Fig. 2 c). In Last case we have more intensive generated of microstructures.

For light absorption on unstable centers (amorphous semiconductors) time characteristics haven't large observable influence on formation of irreversible changes in semiconductors. Here integral dose of irradiation has general meaning; therefore in this case photochemical ionizing processes give basic contribution and processes of radiated relaxation are neglected.

With including of light reflection data of Table 1 and Table 2 must be increased on 20-30 percents for regimes of irradiation the Neodimium laser (both regimes) and 250 percents for eximer laser irradiation (reflectance of eximer laser radiation is equaled 60 percents) [1, 2].

In addition we must remember that Ruby laser radiation for crystalline silicon has absorbance on order less as for amorphous, therefore for short regimes of irradiation the processes of bonds breakage may give more influence as for case of Nd-laser irradiation. Polycrystalline layer may include various crystalline phases. We can select condition of irradiation with creation on surface of silicon the nanostructures with various its fourth crystallographic modifications.

The role of irradiated atmosphere on formation of laser-induced surface nanostructures is shown in Fig. 2, Fig.3 and in [17]. An oxidation processes are smooth out the surface (Fig. 2). The decreasing of oxygen concentration is caused the more intensive growth of microcolumns (Fig. 2 b)) and nanocolumns (Fig. 3).

The influence of pulse numbers on generated the surface interferograms on titanium was received in [13, 14, 1, 2]. The cascade model may be used for the explanation of these experimental data of [13, 14]. Titanium has two phases: hexagonal and body-centered cubic [27]. But after heating the titanium to 882,5°C it has only cubic phase [27]. According to cascade model peaks of proper surface columns must have hexagonal symmetry, but its generation is attended with oxidation processes. Therefore the intensities of creation the surface structures are various for two groups of pulses: for second group (70 – 110 pulses) is more intensive process as for first group of pulse (10 – 50 pulses) [13]. Among these regimes of irradiation may be receive the doubling of period of interference pattern [13].

This method was used for the explanation of the experimental data about laser-induced transformations in various allotropic phases of carbon, included diamond, graphite, fullerenes and other [2] too.

We can use cascade model for explanations o experimental data for polymers. The main characteristic of necessary polymers are represented in Table 8 [20, 28-32].

Table 8. Some characteristics of polymers [20, 28-32].

Material	M _w (g/mol)	M _n (g/mol)	M _{1bl} (g/mol)	n _w	n _n	n _{wbond}	n _{nbond}	ρ (g/cm ³)	α ₂₁₃ (10 ³ cm ⁻¹)	α ₂₆₆ (10 ³ cm ⁻¹)
PET	27600	18800	232	119	81	2925	2025	1,39	38	18
PTT	42000	21000	250	168	84	4704	2352	1,35	52	26
PC	64900	30000	254	256	118	9216	4248	1,20	193	18
PVDF	288000	64000	64	4500	1000	31500	7000	1,76	0,6	0,4
PS	500000	300000	104	4808	2885	76928	46154	1,10	100	40

Where M_w – weight average molecular weight, M_n – number average molecular weight, M_{1bl} – molecular weight of one block of polymer, n_w – number of blocks for M_w, n_n – number of blocks for M_n, n_{wbond} – number of chemical bonds for M_w, n_{nbond} – number of chemical bonds for M_n, ρ - the density of proper polymer, α_i – linear absorption indexes for proper wavelength.

Number of blocks was received from formula

$$n_i = \frac{M_i}{M_{1bl}}, \quad i \in (w, n). \tag{6}$$

Number of bonds in macromolecule n_{ibond} may be determined as

$$n_{ibond} = n_i \cdot m_j, \quad i \in (w, n). \tag{7}$$

Where m_j is the number of chemical bonds in molecule of j block

The energies of corresponding chemical bonds, which are main elements of polymers of Table 8, which are represented in Table 9.

Table9. Energies and lengths of covalent chemical bonds, which are main elements of using polymers.

Bond	C-C	C=C	C≡C	C-H	C-H	C-O	C=O	C-F	C-Cl	C-Br	C-N	O-H	N-H
E_i, eV	3,61	6,44	8,46	4,30	4,52	3,57	7,35	5,01	3,44	2,87	3,04	4,78	4,04
L_i, nm	0,154	0,133	0,120	0,110	0,107	0,143	0,121	0,136	0,176	0,194	0,147	0,096	0,101

Densities of macromolecules may be determined with help formula

$$N_{imol} = \frac{\rho N_A}{M_i}, \quad i \in (w, n). \tag{2a}$$

Densities of proper bonds is equaled

$$N_{jb} = \frac{n_i}{n_{ij}} N_{i\Sigma b} = \frac{n_i}{n_{ij}} n_{ibond} N_{imol} = \frac{n_j}{n_{ij}} \frac{\rho N_A}{M_{imol}}, \quad i \in (w, n), \tag{8}$$

where n_j – number of corresponding bonds in block of j -molecule.

The densities of macromolecules and bonds with energy less as 5, 8 eV are represented in the Table 10.

Table10. The densities of macromolecules and its bonds (cm^{-3}).

Material		PET	PTT	PC	PVDF	PS
N_{mol}	w	$3,0 \cdot 10^{19}$	$1,9 \cdot 10^{19}$	$1,0 \cdot 10^{19}$	$3,7 \cdot 10^{18}$	$1,3 \cdot 10^{18}$
	n	$4,4 \cdot 10^{19}$	$3,9 \cdot 10^{19}$	$2,4 \cdot 10^{19}$	$1,7 \cdot 10^{19}$	$2,2 \cdot 10^{18}$
$N_{\Sigma b}$	w	$8,8 \cdot 10^{22}$	$9,1 \cdot 10^{22}$	$1,1 \cdot 10^{23}$	$1,2 \cdot 10^{22}$	$1,0 \cdot 10^{23}$
	n	$8,9 \cdot 10^{22}$	$9,1 \cdot 10^{22}$	$1,0 \cdot 10^{23}$	$1,2 \cdot 10^{22}$	$1,0 \cdot 10^{23}$
C-C	w	$2,2 \cdot 10^{22}$	$2,3 \cdot 10^{22}$	$3,1 \cdot 10^{22}$	$5,1 \cdot 10^{21}$	$2,5 \cdot 10^{22}$
	n	$2,2 \cdot 10^{22}$		$2,8 \cdot 10^{22}$		
C-H	w	$1,0 \cdot 10^{22}$	$1,4 \cdot 10^{22}$	$3,1 \cdot 10^{22}$	$3,4 \cdot 10^{21}$	$5,0 \cdot 10^{22}$
	n	$1,0 \cdot 10^{22}$		$2,8 \cdot 10^{22}$		
C-H	w	$1,0 \cdot 10^{22}$	$1,4 \cdot 10^{22}$	$3,1 \cdot 10^{22}$	$3,4 \cdot 10^{21}$	$5,0 \cdot 10^{22}$
	n	$1,0 \cdot 10^{22}$		$2,8 \cdot 10^{22}$		
C-O	w	$2,5 \cdot 10^{21}$	$4,6 \cdot 10^{21}$	$6,1 \cdot 10^{21}$	-	-
	n	$2,5 \cdot 10^{21}$		$5,6 \cdot 10^{21}$		
C-F					$3,4 \cdot 10^{21}$	

The corresponding to Table 10 summarized a volume densities of energy for our polymers are represented in Table 11.

Table 11. A volume densities of energy for our polymers E_{vol} ($10^3 J/cm^3$).

Material	PET	PTT	PC	PVDF	PS
C-C	12,7	13,3	17,0	6,9	14,4
C-H	6,9	9,6	20,3	2,3	34,4
C-H	7,2	10,1	21,3	2,5	38,3
C-O	1,4	2,6	3,3	-	-
C-F				2,7	

The surface densities of energy may be received with help formula

$$E_{sur} = E_{vol}/\alpha. \tag{9}$$

Corresponding data for wavelength 213 and 266 nm are represented in Table 12.

Table 12. The surface densities of energy for wavelength 213 and 266 nm E_{sur} (J/cm^2).

Material	PET		PTT		PC		PVDF		PS	
	213	266	213	266	213	266	213	266	213	266
C-C	0,334	0,706	0,256	0,512	0,088	0,944	11,5	17,25	0,144	0,36
C-H	0,182	0,383	0,185	0,370	0,105	1,128	3,833	5,75	0,344	0,86
C-H	0,189	0,400	0,194	0,388	0,110	1,183	4,167	6,25	0,383	0,958
C-O	0,036	0,078	0,050	0,100	0,017	0,183	-	-		
C-F							4,5	6,75		

Now we made comparative analysis and experimental data [20-22]. Real regimes of irradiation, which are used for the crystallization of PVDF and PTT (Fig. 6), are smaller as in Table 12. It may be explain in next way. Data of Table 12 were received for the next approximation; regime of saturation the excitation for all chemical bonds of corresponding type. Really for the phase transformations we must have lesser number of breakage chemical bonds. In this case we must take into account one, two and other numbers of bonds as for silicon. But for the case of PTT estimated data are equivalence with experimental data. In this case we have phase transition from amorphous to crystalline phase. For PVDF phase transformations are more soft: from semicrystalline phase to other, including the increasing of sizes initial crystals (Fig. 6 (d) – (f)). Therefore intensity of irradiation in this case is smaller as data of Table 12. Thus, the cascade theory of excitation of corresponding chemical bonds in the regime of saturation the excitation may be used for the modeling the laser-induced phase transformations in polymers too. The optical-induced phase transformations in polymers must be connected with self-absorption range of light. For the case of polymers the time of irradiation hasn't great value on finish result, basic value has integral fluence of light. Phe polymers are more complex compounds as semiconductors and metals with covalent bonds and it has more widely spectrum of phase state from liquid to crystals [28-32]. Therefore using of cascade model of excitation of corresponding type and number of the chemical bonds in the regime of saturation the excitation for the modeling laser-induced phase transformations allow help to receive the regimes of laser irradiation, which must be used for the creation the corresponding phase transformations in irradiated matter.

The influence of polarization on formation laser-induced surface structures may be explain with help Vladimir Makin polariton-plasmon model [7]. Results of Fig. 5 show that various linear polarization are generated varius structure and this structures are parallel to direction of vector of polarization. In [20] was shown that circular polarization of laser radiation allow receiving the circular surface structures. More detail analysis of this question is represented in [7].

4. CONCLUSION

1. The experimental data of creation surface laser-induced structures on silicon, germanium, titanium, polymers and other materials are represented, modeled and discussed.
2. Short comparative analysis of models, which are used for the explanation of represented experimental data are made.
3. Cascade model of step-by-step excitation of proper chemical bonds in the regime of saturation the excitation is observed.
4. We show that cascade model allows explaining basic peculiarities of represented experimental data for silicon and germanium, including generation of new crystalline phases.
5. We accented that creation of LIPPS must be modeled with help V. Makin polariton-plasmon model.
6. Euristic criteria of estimation the efficiencies of using the laser radiation for the represented experimental data are formulated and used f or silicon.
7. The influence of mechanisms of absorption the laser radiations and conditions of laser irradiation on formation are shown and discussed.
8. The principal possibility of using the cascade model of excitation the corresponding chemical bonds in the regime of saturation the excitation is shown for five polymers and it allow to explaine experimental data of laser-induced phase transformations in PTT.

REFERENCES

- [1] Trokhimchuck P. P. (2020) *Relaxed Optics: Modeling and Discussions*. Lambert Academic Publishing, Saarbrücken.
- [2] Trokhimchuck P. P. (2016) *Relaxed Optics: Realities and Perspectives*. Lambert Academic Publishing, Saarbrücken.
- [3] Trokhimchuck P.P. (2015) *Relaxed Optics: Necessity of Creation and Problems of Development*. IJARPS, Vol. 2, Is. 3, 22-33
- [4] Trokhimchuck P. P. (2018) Problems of modeling the phase transformations in Nonlinear and Relaxed Optics (review). IJERD, Vol.14, Is.2, 48-61.
- [5] Shen Y. R. (2002) *Principles of nonlinear optics*, Wiley Interscience, Ney-York a. o.
- [6] Medvid' A. Nano-cones Formed on a Surface of Semiconductors by Laser Radiation: Technology, Model and Properties/ *Nanowires Science and Technology* ed. Nicoletta Lupu. – Vukovar: Inech, 2010. – P.61–82.
- [7] Makin V. S. (2013) Peculiarities of the formation the ordered micro and nanostructures in condensed matter after laser excitation of surface polaritons modes. D. Sc. Thesis. State university of information technologies, mechanics and optics, Saint-Petersburg: 2013. (In Russian)
- [8] Pedraza A. J., Fowlkes J. D. and Lowndes D. H. (1999) Silicon microcolumn arrays growth by nanosecond pulse laser irradiation. *Appl. Phys. Lett.*, Vol. 74, Is. 10, 2222-2224.
- [9] Pedraza A. J., Guan Y. F., Fowlkes J. D., Smith D. A. and Lowndes D. H. (2004) Nanostructures produced by ultraviolet laser irradiation of silicon. I. Rippled structures. *J. Vac. Sc. @ Techn. B.*, Vol. 22, №10, 2004. 2823-2835.
- [10] Shen M., Carey J. E., Crouch C. H., Kandyla M., Stone H. A. and Mazur E. (2008) High-density regular arrays of nano-scale rods formed on silicon surfaces via femtosecond laser irradiation in water. *Nanoletters*, Vol. 8, Is. 7, 2087-2091.
- [11] Costache E., Kouteva-Anguiriva S., Reif J. (2004) Sub-damage-threshold femtosecond laser ablation from crystalline Si: surface nanostructures and phase transformations. *Appl. Phys. A*, Vol. 79, 1429 – 1432.
- [12] Hirata K., Haraguchi K. (2008) Crystallization of fused silica surfaces by ultra-violet laser irradiation. *J. Appl. Phys.*, Vol. 104, No.12, 2008. 1–4.
- [13] Tsukamoto M., Asuka K., Nakano N., Hashida M., Ratto M., Abe N., Fujita M. (2006) Periodic microstructures produced by femtosecond laser irradiation on titanium plate. *Vacuum*, Vol. 80, 1346-1350.
- [14] Landis E.C., Phillips K.C., Mazur E., Friend C.M. (2012) Formation of nanostructured TiO₂ by femtosecond laser irradiation of titanium in O₂. *J. Appl. Phys.*, Vol. 112, Is.6, 063108, 2012, 1–5.
- [15] Bonse J., Krüger J., Höhm S., Rosenfeld A. (2012) Femtosecond periodic laser-induced structures. *Journal of Laser Applications*, Vol. 24, Is. 4, 042006-1 – 042006-7.
- [16] Bonse J., Rosenfeld A., Krüger J. (2009) On the role of surface plasmon polaritons in the formation of laser-induced periodic surface structures upon irradiation of silicon by femtosecond-laser pulses. *J. Appl. Phys.*, Vol. 106, Is.10, 104910, 1–5.
- [17] Ebert T., Neumann N. W., Abel T., Schaumann G., Roth M. (2017) Laser-induced microstructures on silicon for laser-driven acceleration experiments. *High Power Laser Science and Engineering*, vol. 5, e13, 6.
- [18] Agida S. N., Brabazon D., Naher S. (2013) An investigation of phase transformation and crystallinity in laser surface modified H13 steel. *Appl. Phys. A.*, Vol. 110, 673-678.
- [19] Birnbaum M. (1965) Semiconductor surface damage produced by Ruby Laser. *J. App. Phys.*, Vol. 36, Is.11, 3688–3689.
- [20] Rebollar E., Peres S., Hernandez J. J., Martin-Fabiani I., Rueda D. R., Ezguerra T. A., Castillejo M. Assesment (2011) Formation Mechanism of Laser-Induced Periodic Surface Structures on Polymer Spin-Coated Films in Real and Reciprocal Space. *Langmuir*, Vol 27, 5596 – 5606.
- [21] Rebollar E., Castillejo M., Ezguerra T. A. (2015) Laser Induced Periodic Surface Structures on Polymer Films (2015) *European Polymer Journal*. Accepted manuscript, 1-32
- [22] Heitz J., Reisinger B., Fahrner M., Romanin C., Siegel J., Svorcik V. (2012) Laser-Induced Periodic Surface Structures (LIPSS) on Polymer Surfaces. *ICTON*, Tu.B5.2, 1-4.
- [23] Philips J.C. (1981) Metastable honeycomb model of laser annealing. *Journal of Applied Physics*, No.12, Vol. 52, 7397-7402.
- [24] Rayleigh (J. W. Strutt). (1916) On convective currents in a horizontal layer of fluid then the higher temperature is on the under side. *Philosoph. Mag.*, Vol. 32, 529-546.
- [25] Chandrasekar S. (1961) *Hydrodynamic and Hydromagnetic Stability*. Dover Publications, New York
- [26] Haken H. *Synergetics*. (1977) Springer-Verlag, Berlin-Heidelberg-New York

- [27] Donachie M. J. (2000) Titanium: A Technical Guide Materials Park, Ohio
- [28] Cotterill R. (1989) The Cambridge Guide to the Material World, Cambridge University Press, Cambridge.
- [29] Bartenev V. M., Frenkel S. Ya. (1990) Polymer Physics, Chemistry, Leningrad (in Russian)
- [30] Khohlov A. R., Kuchanov S. I. (2000) Lectures Physical Chemistry of Polymers, Mir, Moscow (in Russian)
- [31] Odian G. G. (1974) The Foundations of Polymer Chemistry, Mir, Moscow (In Russian)
- [32] The encyclopaedia of polymers, vol. 1- 3 (1972-1977), Soviet encyclopaedia, Moscow (In Russian)

Citation: *Petro P. Trokhimchuck, (2020). Some Peculiarities the Modeling the Surface Processes of Relaxed Optics. International Journal of Advanced Research in Physical Science (IJARPS) 7(5), pp.3-16 2020.*

Copyright: © 2020, Authors, This is an open-access article distributed under the terms of the Creative Commons Attribution License, which permits unrestricted use, distribution, and reproduction in any medium, provided the original author and source are credited.